Strength of anisotropy in a granular material: Linear versus nonlinear contact model

Luigi La Ragione, Marica Gammariello, and Giuseppina Recchia
Dipartimento di Scienze dell'Ingegneria Civile e dell'Architettura, Politecnico di Bari, 70125 Bari, Italy
(Received 24 September 2016; revised manuscript received 17 November 2016; published 19 December 2016)

In this paper, we deal with anisotropy in an idealized granular material made of a collection of frictional, elastic, contacting particles. We present a theoretical analysis for an aggregate of particles isotropically compressed and then sheared, in which two possible contacts laws between particles are considered: a linear contact law, where the contact stiffness is constant; and a nonlinear contact law, where the contact stiffness depends on the overlapping between particles. In the former case the anisotropy observed in the aggregate is associated with particle arrangement. In fact, although the aggregate is initially characterized by an isotropic network of contacts, during the loading, an anisotropic texture develops, which is measured by a fabric tensor. With a nonlinear contact law it is possible to develop anisotropy because contacting stiffnesses are different, depending on the orientation of the contact vectors with respect to the axis of the applied deformation. We find that before the peak load is reached, an aggregate made of particles with a linear contact law develops a much smaller anisotropy compared with that of an aggregate with a nonlinear law.

DOI: 10.1103/PhysRevE.94.062904

I. INTRODUCTION

A granular material is made of a collection of frictional, elastic, contacting particles. Its behavior is rather complex because the macro response of the aggregate (the average stress over all particles), due to an applied average deformation, depends on how particles deform, slide, and delete. In their motion, particles typically deviate from the applied macroscopic deformation in order to satisfy force and moment equilibrium [1,2]. At contact level, the interaction force between particles is often represented by a noncentral force: a normal component that follows the Hertz law where a nonlinear relation between force and displacement is employed, and a tangential force that is simplified by an elasto-frictional sliding relation. This hypothesis is supported by experimental evidences [3–6] and, consequently, both theoretical models and numerical simulations, based upon a nonlinear contact law, are available to predict the behavior of such an aggregate [7,8]. Numerical simulations, based upon the Distinct Element Method first employed by [9], also provide a large number of data that can be useful to understand the behavior of the aggregate from the micro-mechanical point of view and to test theoretical models. A better statistics of key parameters of the aggregate is achieved when a large number of particles is taken at expenses of a greater computational time.

It is possible to deal with a simpler computational scheme if we consider a linear contact law between force and displacement [10]. This is a proper assumption if we have an aggregate of disks [11] while, in case of aggregate of spheres, the linear contact law is a simplification justified to deal with faster computation [12]. Similar arguments are introduced when the linear contact law is taken in the theoretical models [13,14].

At this point we wonder how the linear model differs from the nonlinear model and if this simplification is reasonable. We attempt to answer this question by focusing on anisotropy. We present results obtained by means of a simple theoretical model in which we show that the choice of a contact model at expense of the other can be questionable. We study a monotonic loading condition applied to an aggregate of elastic, frictional particles: an isotropic compression followed by a uni-axial compression along the vertical axis, $y_3 = \mathbf{h}$. The initial, isotropic, stressed aggregate becomes transversely isotropic when sheared. We compare the strength of anisotropy in two aggregates: the first is characterized by a linear contact model, the second by a nonlinear contact model. We restrict our attention to a regime of deformation in which it is plausible to associate with the first aggregate anisotropy in the contact network (fabric) while with the second aggregate anisotropy in the contact stiffness. The result is that aggregates of particles with a linear contact model develop a strength of anisotropy much smaller compared to that associated with aggregates where a nonlinear model is employed. Because anisotropy is crucial in granular material to make a quantitative prediction of dilatancy, shear bands, waves propagation, we conclude that the present results can offer some understanding about the limitation of one model with respect to the other.

II. THEORY

A. Kinematics

We consider a dense aggregate of N identical, frictional elastic spheres with diameter d, isotropically compressed and then sheared at constant pressure. The kinematics of contacting particles, A and B, is given in terms of the increments $\dot{\mathbf{c}}^{(A)}$ and $\dot{\mathbf{c}}^{(B)}$ in the translations of the centers of the two spheres and the increments $\dot{\omega}^{(A)}$ and $\dot{\omega}^{(B)}$ in the rotations about their centers, so that

$$\dot{u}_i^{(BA)} = \dot{c}_i^{(B)} - \dot{c}_i^{(A)} - \tfrac{1}{2}\varepsilon_{ijk}\left(\dot{\omega}_j^{(B)} + \dot{\omega}_j^{(A)}\right)d_k^{(BA)}, \qquad (1)$$

where $\dot{\mathbf{u}}^{(BA)}$ is the incremental contact displacement and $\mathbf{d}^{(BA)}$ is the vector from the center of particle A to the center of particle B. The rectangular Cartesian components of the unit vector $\hat{\mathbf{d}}$ are $(\sin\theta\cos\varphi, \sin\theta\sin\varphi, \cos\theta)$, where θ is the polar angle from the axis of symmetry (see Fig. 1).

It is possible to describe the kinematics of contacting particles through averages quantities and fluctuations in order to consider force and moment equilibrium locally [1,2]. Here we work in a simpler context and we neglect fluctuations in

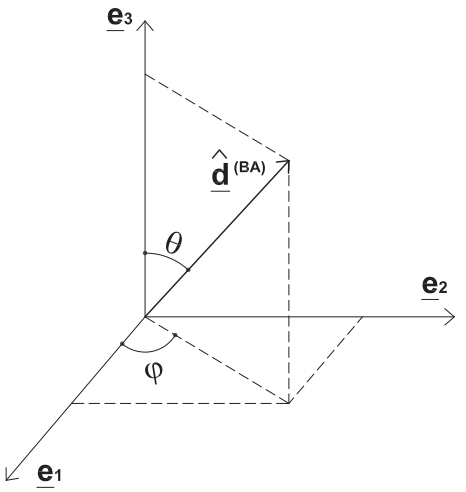

FIG. 1. Cartesian reference.

particle deformations so the relative incremental displacement of the centers is given simple by

$$\dot{c}_i^{(B)} - \dot{c}_i^{(A)} = (D_{ij} + W_{ij}) d_j^{(BA)}, \tag{2}$$

where **D** and **W** are, respectively, the symmetric and antisymmetric parts of the increment in the average deformation gradient. The rate of the average rotation of the spheres about their centers is equal to $\boldsymbol{\Omega}^{\times}$, the axial vector of the skew-symmetric tensor $\boldsymbol{\Omega}$, so

$$\dot{\omega}_j^{(A)} + \dot{\omega}_j^{(B)} = 2\Omega_j^{\times}. \tag{3}$$

The increment average rotation based upon the displacements of the particle centers is different from the increment average spin about the centers as anisotropy develops [15]. Since particles are constrained to move with the average deformation, local force and moment equilibrium are identically satisfied once the symmetry of the average stress is imposed. When anisotropy develops, **W** can differ from $\boldsymbol{\Omega}$ to guarantee global moment equilibrium.

B. Contact force

The increment $\dot{\mathbf{F}}^{(BA)}$ in the contact force exerted by particle B on particle A is

$$\dot{F}_i^{(BA)} = K_{ij}^{(BA)} \dot{u}_j^{(BA)}, \tag{4}$$

where $\mathbf{K}^{(BA)}$ is the contact stiffness

$$K_{ij}^{(BA)} = K_N^{(BA)} \hat{d}_i^{(BA)} \hat{d}_j^{(BA)} + K_T^{(BA)} \left(\delta_{ij} - \hat{d}_i^{(BA)} \hat{d}_j^{(BA)}\right). \tag{5}$$

The normal $K_N^{(BA)}$ and tangential $K_T^{(BA)}$ contact stiffnesses are functions of the normal component ρ of the compressive displacement of the centers of the particles, the diameter d of the spheres, and their material properties

$$K_N^{(BA)} = \frac{\mu d^{1/2}}{(1-\nu)} \rho^{1/2} \tag{6}$$

and

$$K_T^{(BA)} = \frac{2\mu d^{1/2}}{(2-\nu)} \rho^{1/2}, \tag{7}$$

where μ and ν are the shear modulus and Poisson's ratio of the particles. While the incremental displacement in the centers of contacting particles is given by the averages of the increments, the normal component ρ of the compressive displacement is

$$\rho = -\hat{d}_i^{(BA)} E_{ij} d_j^{(BA)}. \tag{8}$$

This is how the stiffness depends upon the existing average strain **E**. As the aggregate is first compressed isotropically and then subjected to a deviatoric strain, according to [16], we write

$$\rho = \frac{d}{3}(b + c\cos^2\theta), \tag{9}$$

where $b = \Delta - 2\gamma$ and $c = 6\gamma$, with $2\gamma \equiv E_{11} - E_{33}$, $\Delta = -(2E_{11} - E_{33})$.

C. Incremental stress

Given $\dot{\mathbf{F}}^{(BA)}$, the incremental average stress $\dot{\sigma}$ is

$$\dot{\sigma}_{ij} = \frac{n}{2} \int_{\alpha} f(\hat{\mathbf{d}}) K_{ik} d_j d_l d\Omega (D_{kl} + R_{kl}), \tag{10}$$

where the integration is over all solid angles Ω, $R_{kl} = W_{kl} - \Omega_{kl}$, n is the number of particles per unit volume, and $f(\hat{\mathbf{d}})$ is the contact distribution function defined so that $f(\hat{\mathbf{d}})d\Omega$ is the number of contacts in the element of solid angle $d\Omega = \sin\theta d\theta d\varphi$ centered at $\hat{\mathbf{d}}$. For an initial, isotropic distribution of contacts, $f(\hat{\mathbf{d}}) = k_0/4\pi$, where k_0 is the coordination number in that state. Nevertheless an aggregate can be characterized by an initial anisotropy; this often occurs in a laboratory sample, e.g., pluviation, vibration, tamping [17]. Under these circumstances an applied isotropic compression would induce a volume strain Δ along with a shear strain γ [18] and the contact distribution would not be isotropic. However, we avoid such a condition and we refer to numerical simulations where it is possible to deal with an almost initial isotropic aggregate.

D. Effective moduli

1. Nonlinear contact model

In order to calculate the effective moduli we need to carry out the integral in Eq. (10). Because our goal is to compare the anisotropy associated with the contact stiffness with that associated with the contact network we restrict our interest in the range of deformation where deletion is negligible and the geometrical network of the contacts remains almost isotropic. This assumption is corroborated by numerical simulations where, in the small strain regime, only weakly contacts experience deletion [19]. So,

$$\dot{\sigma}_{ij} = \frac{n}{2} d^2 \int_{\Omega} f(\hat{\mathbf{d}}) K_{im} \hat{d}_n \hat{d}_j d\Omega (D_{mn} + R_{mn}) \tag{11}$$

and if we neglect the term proportional to the difference in the stiffness (we take $\nu = 0.2$ for typical glass beads)

$$\dot{\sigma}_{ij} = \frac{n}{2} d^2 \int_{\Omega} f(\hat{\mathbf{d}}) K_T \delta_{im} \hat{d}_n \hat{d}_j d\Omega (D_{mn} + R_{mn}) \tag{12}$$

or

$$\dot{\sigma}_{ij} = a \int_{\Omega} f(\hat{\mathbf{d}}) (b + c\cos^2\theta)^{1/2} \delta_{im} \hat{d}_n \hat{d}_j d\Omega (D_{mn} + R_{mn}), \tag{13}$$

where $a = n\mu d^3/[3^{1/2}(2-\nu)]$. Because we assume a fixed contact geometry during the loading, the anisotropy is only present in the material through the contact stiffness. The result of integration for the stress is in Appendix A, with $f(\hat{\mathbf{d}}) = \hat{k}/(4\pi)$ where $\hat{k}$ is the coordination number at given stressed state. We have

$$\dot{\sigma}_{ij} = A_{ijst} D_{st} \tag{14}$$

with

$$A_{ijst} = \frac{\hat{ak}}{8}\left(\delta_{is}\delta_{tj} + \delta_{it}\delta_{sj}\right) I_1 + \frac{\hat{ak}}{4}\frac{(2I_2 - I_1)^2}{(2I_2 + I_1)} h_t h_i h_s h_j - \frac{\hat{ak}}{8}\frac{I_1(I_1 - 2I_2)}{(2I_2 + I_1)} \times (\delta_{is}h_t h_j + \delta_{it}h_s h_j + \delta_{js}h_t h_i + \delta_{jt}h_s h_i) \tag{15}$$

and

$$I_1 = \int_0^\pi (b + c\cos^2\theta)^{1/2} \sin^3\theta d\theta, \tag{16}$$

$$I_2 = \int_0^\pi (b + c\cos^2\theta)^{1/2} \cos^2\theta \sin\theta d\theta. \tag{17}$$

The shear modulus in the isotropic plane, A_{1212}, and that associated with the axis of anisotropy $\mathbf{h}$, A_{1313}, are

$$A_{1212} = \frac{\hat{k}a}{8} I_1 \tag{18}$$

and

$$A_{1313} = \frac{\hat{k}a}{2}\frac{I_1 I_2}{(2I_2 + I_1)}. \tag{19}$$

E. Linear contact model

In the case of the linear contact model the stress is

$$\dot{\sigma}_{ij} = \frac{n}{2} d^2 \int_\Omega f(\hat{\mathbf{d}}) K_{im} \hat{d}_n \hat{d}_j d\Omega (D_{mn} + R_{mn}), \tag{20}$$

where anisotropy enters in the contact distribution function

$$f(\hat{\mathbf{d}}) = \frac{\hat{k}}{4\pi}[(1-\epsilon) + 3\epsilon\left(h_i \hat{d}_i\right)^2], \tag{21}$$

where $\mathbf{h} \equiv \mathbf{y}_3$ is the axis of anisotropy and ϵ, positive and less than 1, is the strength of anisotropy [16]. The contact stiffnesses are constant and equal to the initial, isotropic value. That is, $K_N^{(BA)}$ and $K_T^{(BA)}$ are given by Eqs. (6) and (7) when $\rho = d\Delta_0/3$ and with $\nu = 0.2$ we have $K_N \simeq 1.1 K_T$. We could have taken different values for the constant contact stiffnesses [20] but this is a simple way to compare the two type of anisotropies. So,

$$K_{im} = \frac{\mu d}{(1-\nu)}\left(\frac{\Delta_0}{3}\right)^{1/2} \hat{d}_i \hat{d}_m + \frac{2\mu d}{(2-\nu)}\left(\frac{\Delta_0}{3}\right)^{1/2} (\delta_{im} - \hat{d}_i \hat{d}_m) \tag{22}$$

and the incremental stress becomes

$$\dot{\sigma}_{ij} = \frac{n\mu d^3}{2(1-\nu)}\left(\frac{\Delta_0}{3}\right)^{1/2} \int_\Omega f(\hat{\mathbf{d}}) \hat{d}_i \hat{d}_m \hat{d}_n \hat{d}_j d\Omega D_{mn} + \frac{n\mu d^3}{(2-\nu)}\left(\frac{\Delta_0}{3}\right)^{1/2} \times \int_\Omega f(\hat{\mathbf{d}})(\delta_{im} - \hat{d}_i \hat{d}_m)\hat{d}_n \hat{d}_j d\Omega (D_{mn} + R_{mn}). \tag{23}$$

Again, we neglect the contribution associated with the difference between normal and tangential stiffness, so the incremental stress is given by

$$\dot{\sigma}_{ij} = \frac{\hat{k}a\Delta_0^{1/2}}{4\pi}(D_{in} + R_{in}) \int_\Omega [(1-\epsilon) + 3\epsilon(h_q \hat{d}_q)^2] \hat{d}_n \hat{d}_j d\Omega. \tag{24}$$

The symmetry of the stress implies

$$\varepsilon_{kij}\dot{\sigma}_{ij} = 0 \tag{25}$$

or

$$\varepsilon_{kmj} \int_\Omega [(1-\epsilon) + 3\epsilon(h_q \hat{d}_q)^2] \hat{d}_n \hat{d}_j d\Omega (D_{mn} + R_{mn}) = 0. \tag{26}$$

In Appendix B we report details of the calculation. The result is

$$R_{mn} = \frac{3\epsilon}{5+\epsilon} \varepsilon_{msn}\varepsilon_{spj} h_k h_j D_{pk} \tag{27}$$

and the incremental stress, Eq. (24), linear in ϵ, is

$$\dot{\sigma}_{ij} = a\hat{k}\Delta_0^{1/2}\frac{5-2\epsilon}{30}(\delta_{im}\delta_{nj} + \delta_{in}\delta_{mj})D_{mn} + a\hat{k}\Delta_0^{1/2}\frac{\epsilon}{10} \times (\delta_{im}h_j h_n + \delta_{jm}h_i h_n + \delta_{in}h_j h_m + \delta_{jn}h_i h_m) D_{mn}. \tag{28}$$

If the incremental stress is written in compact form as

$$\dot{\sigma}_{ij} = B_{ijnm} D_{nm},$$

then the shear moduli are

$$B_{1212} = a\hat{k}\Delta_0^{1/2}\frac{5-2\epsilon}{30} \tag{29}$$

and

$$B_{1313} = a\hat{k}\Delta_0^{1/2}\frac{5+\epsilon}{30}. \tag{30}$$

F. Comparison

In the initial, isotropic state, $b = \Delta_0$ with $c = 0$ or $\epsilon = 0$, the shear modulus is ($A_{1212}^{\text{iso}} = A_{1313}^{\text{iso}} = B_{1212}^{\text{iso}} = B_{1313}^{\text{iso}} = G$)

$$G = ak_0\frac{\Delta_0^{1/2}}{6}, \tag{31}$$

where k_0 is the initial coordination number and Δ_0 is the volume associated with the initial, isotropic state. In both the nonlinear and linear contact model, we take the evolution of the shear moduli to quantify the strength of anisotropy. In particular, the shear moduli derived in the nonlinear model, Eqs. (18) and (19) evolve during the loading with γ/Δ_0 which is also a function of Δ/Δ_0; the shear moduli derived in the

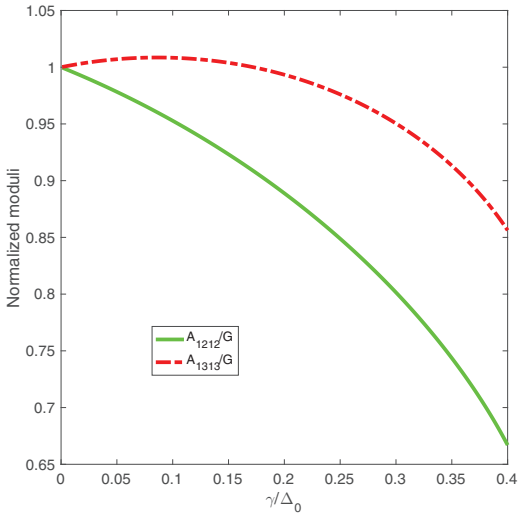

FIG. 2. Evolution of the shear moduli for the nonlinear contact model.

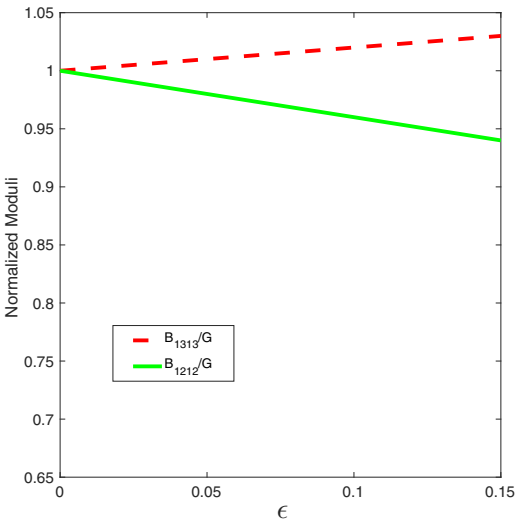

FIG. 3. Evolution of the shear moduli for the linear contact model.

linear model, Eqs. (29) and (30), evolve during the loading with ϵ. In the former model, we use the relation between the volume strain and the shear strain provided by [16], or its approximate version [21]

$$\frac{\Delta}{\Delta_0} = 1 - 0.8\left(\frac{\gamma}{\Delta_0}\right)^2 \tag{32}$$

to write Eqs. (18) and (19) as a function of one parameter, γ/Δ_0. The nonlinear contact model is characterized by the following normalized moduli:

$$\frac{A_{1212}}{G} = \frac{3\hat{k}}{4k_0}\frac{I_1}{\Delta_0^{1/2}}, \tag{33}$$

$$\frac{A_{1313}}{G} = \frac{3\hat{k}}{k_0\Delta_0^{1/2}}\frac{I_1 I_2}{2I_2 + I_1}. \tag{34}$$

We plot both in Fig. 2, where γ/Δ_0 is limited within the pre-peak region [16].

For the linear contact model we have

$$\frac{B_{1212}}{G} = \frac{\hat{k}}{k_0}\frac{5-2\epsilon}{5} \tag{35}$$

and

$$\frac{B_{1313}}{G} = \frac{\hat{k}}{k_0}\frac{5+\epsilon}{5} \tag{36}$$

which are shown in Fig. 3. We limit our attention to values of ϵ between 0 and 0.15 which are reasonable in the pre-peak region. In both the linear and nonlinear models we neglect contact deletion and we simply focus on anisotropy in the stiffness (nonlinear case) and anisotropy in the contact orientations (linear case). The investigation could be extended to a larger range of deformation where deletion occurs; however, in the present limits, we are able to isolate the two mechanisms responsible for the anisotropy: anisotropy in the stiffness (nonlinear model) and contact distribution (linear model).

Another interesting parameter associated with the contact network is the fabric tensor [22] defined as

$$F_{ij} = \int_\Omega \tilde{f}(\hat{\mathbf{d}})\hat{d}_i\hat{d}_j d\Omega, \tag{37}$$

where $\tilde{f}(\hat{\mathbf{d}})$ does not contain $\hat{k}$. In the case of anisotropy, with Eq. (21) without $\hat{k}$, the fabric tensor is

$$F_{ij} = \frac{5-2\epsilon}{15}\delta_{ij} + \frac{2}{5}\epsilon h_i h_j. \tag{38}$$

Following [10], in Fig. 4 we plot the deviatoric part of the fabric tensor $F^D = F_{33} - F_{11}$ against ϵ, in the same range as Fig. 3. This measure of anisotropy can be available in numerical simulations and it can be used to infer ϵ. From [7], for example, we derive an upper limit for ϵ to be about 0.15, considering a range of deformation that precedes the highest value in the deviatoric stress (we take $F^D = 0.06$), where

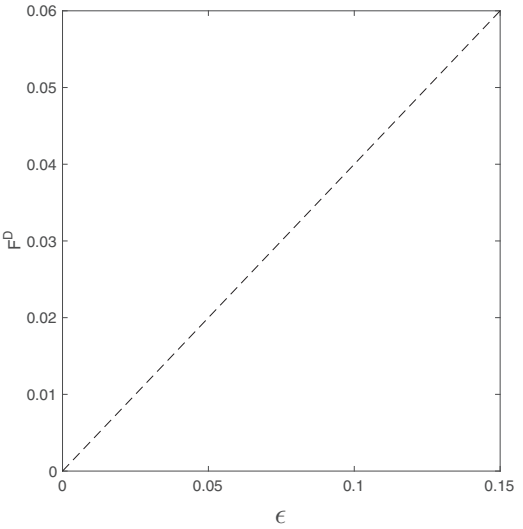

FIG. 4. Evolution of the deviatoric part of the fabric tensor, F^D, with ϵ.

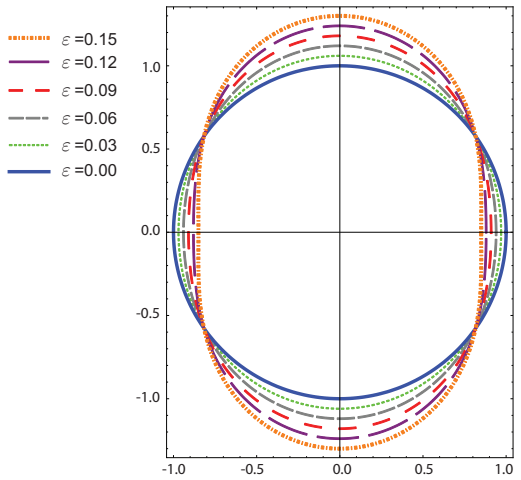

FIG. 5. Rose diagrams with different values of ϵ.

deletion is still limited. In [23,24] we also have information regarding fabric although the authors refer to a frictionless aggregate. These systems of particles represent very peculiar aggregates where the possibility to sustain a shear deformation is limited to a very small range. However we recover from their data [24] $\epsilon \approx 0.05$.

In the range of values of ϵ we plot in Fig. 5 the rose diagrams [6] which highlight the evolution of anisotropy.

Figures 2 and 3 show that the strength of anisotropy associated with the Hertz model (nonlinear) is much stronger than that associated with the linear model. Because of the crucial role that anisotropy plays in the pre-peak region of a granular assembly [25,26], these results suggest that it might not always be appropriate to replace the Hertz law with the linear model.

III. CONCLUSION

By means of a simple theory, we have highlighted a comparison between two different types of contacting models developed in an idealized granular material. We have focused on a typical test where contacting particles deform according to linear and nonlinear laws. In the former case, anisotropy is present because we assume an anisotropic contact distribution; in the latter case, anisotropy is present because contacting stiffnesses are different. We show that, in the regime of deformation that precedes the peak, the Hertz model, which is a natural candidate to model the interaction of spherical particles, develops a much stronger anisotropy compared to the linear model. This suggests that if, on the one hand, the linear model allows a simplification in the calculation, on the other hand it provides a weak anisotropy. The present model, therefore, offers an indication as to whether linear contact interaction is suitable to be employed when the aim is to predict phenomena like shear bands, dilatancy, and wave propagation, where anisotropy plays a crucial role.

ACKNOWLEDGMENTS

L.L.R. is grateful to Gruppo Nazionale della Fisica Matematica (Italy) for partial support of this research.

APPENDIX A: STRESS CALCULATION

The stress is

$$\dot{\sigma}_{ij} = a \int_\Omega f(\hat{\mathbf{d}})(b + c\cos^2\theta)^{1/2}\delta_{im}\hat{d}_n\hat{d}_j d\Omega(D_{mn} + R_{mn}) \tag{A1}$$

and the symmetry requires

$$\varepsilon_{qij}\dot{\sigma}_{ij} = 0 \tag{A2}$$

or

$$0 = \varepsilon_{qij}\int_\Omega f(\hat{\mathbf{d}})(b + c\cos^2\theta)^{1/2}\delta_{im}\hat{d}_n\hat{d}_j d\Omega D_{mn} + \varepsilon_{qij}\int_\Omega f(\hat{\mathbf{d}})(b + c\cos^2\theta)^{1/2}\delta_{im}\hat{d}_n\hat{d}_j d\Omega R_{mn}. \tag{A3}$$

With

$$R_{mn} = \varepsilon_{mkn}w_k, \tag{A4}$$

the symmetry condition, Eq. (A3), becomes

$$\left[\varepsilon_{qij}\int_\Omega f(\hat{\mathbf{d}})(b + c\cos^2\theta)^{1/2}\delta_{im}\hat{d}_n\hat{d}_j d\Omega\right]D_{mn} = L_{kq}w_k, \tag{A5}$$

where

$$L_{kq} = \int_\Omega f(\hat{\mathbf{d}})(b + c\cos^2\theta)^{1/2}\left(\delta_{kq} - \hat{d}_k\hat{d}_q\right)d\Omega. \tag{A6}$$

Because of the symmetry about the axis of anisotropy $\mathbf{h}$, we first consider the following integrals over φ:

$$\left\langle \hat{d}_t\hat{d}_j\right\rangle_\varphi = \frac{1}{2\pi}\int_0^{2\pi}\hat{d}_t\hat{d}_j d\varphi \tag{A7}$$

or

$$\langle \hat{d}_t\hat{d}_j\rangle_\varphi = \tfrac{1}{2}\sin^2\theta\delta_{tj} + \left(\cos^2\theta - \tfrac{1}{2}\sin^2\theta\right)h_t h_j. \tag{A8}$$

So, with $f(\hat{\mathbf{d}}) = \hat{k}/(4\pi)$,

$$L_{kq} = \beta_1\delta_{kq} + \beta_2 h_k h_q, \tag{A9}$$

where

$$\beta_1 = \frac{\hat{k}}{4}\int_0^\pi (b + c\cos^2\theta)^{1/2}(2 - \sin^2\theta)\sin\theta d\theta, \tag{A10}$$

$$\beta_2 = -\frac{\hat{k}}{4}\int_0^\pi (b + c\cos^2\theta)^{1/2}(2\cos^2\theta - \sin^2\theta)\sin\theta d\theta. \tag{A11}$$

With the inverse of tensor **L** and Eq. (A8), Eq. (A5) becomes

$$R_{mn} = Q_{mnst} D_{st}, \tag{A12}$$

where

$$\begin{aligned} Q_{mnst} = {} & \frac{\hat{k}}{4}\beta_1^{-1}\left(\varepsilon_{mkn}\varepsilon_{kst} - \frac{\beta_2}{\beta_1+\beta_2}\varepsilon_{mkn}\varepsilon_{qst}h_k h_q\right) \\ & \times \int_0^{\pi} (b + c\cos^2\theta)^{1/2}\sin^3\theta d\theta \\ & + \frac{\hat{k}}{2}\beta_1^{-1}\left(\varepsilon_{mqn}\varepsilon_{qsz}h_t h_z\right. \\ & \left. - \frac{\beta_2}{\beta_1+\beta_2}\varepsilon_{mkn}\varepsilon_{qsz}h_k h_q h_t h_z\right) \\ & \times \int_0^{\pi} (b + c\cos^2\theta)^{1/2}\left(\cos^2\theta - \frac{1}{2}\sin^2\theta\right)\sin\theta d\theta, \end{aligned} \tag{A13}$$

or

$$\begin{aligned} Q_{mnst} = {} & \frac{\hat{k}}{2}\beta_1^{-1}\varepsilon_{mqn}\varepsilon_{qsz}h_t h_z \\ & \times \int_0^{\pi} (b + c\cos^2\theta)^{1/2}\left(\cos^2\theta - \frac{1}{2}\sin^2\theta\right)\sin\theta d\theta. \end{aligned} \tag{A14}$$

Given Eqs. (16) and (17), we write

$$\beta_1 = \frac{\hat{k}}{4}(2I_2 + I_1) \tag{A15}$$

and

$$\beta_2 = -\frac{\hat{k}}{4}(2I_2 - I_1); \tag{A16}$$

so, tensor **Q** is

$$Q_{mnst} = \frac{2I_2 - I_1}{2I_2 + I_1}\varepsilon_{mqn}\varepsilon_{qsz}h_t h_z. \tag{A17}$$

With Eqs. (A12) and (A17), the incremental stress, Eq. (A1), is written

$$\begin{aligned} \dot{\sigma}_{ij} = {} & \frac{\hat{ak}}{8}(\delta_{is}\delta_{tj} + \delta_{it}\delta_{sj})I_1 D_{st} + \frac{\hat{ak}}{4}\frac{(2I_2 - I_1)^2}{(2I_2 + I_1)}h_t h_i h_s h_j D_{st} \\ & - \frac{\hat{ak}}{8}\frac{I_1(I_1 - 2I_2)}{(2I_2 + I_1)} \\ & \times (\delta_{is}h_t h_j + \delta_{it}h_s h_j + \delta_{js}h_t h_i + \delta_{jt}h_s h_i)D_{st}. \end{aligned} \tag{A18}$$

APPENDIX B

In the case of the linear contact model, the symmetry of the stress implies

$$\varepsilon_{kij}\int_{\Omega}[(1-\epsilon) + 3\epsilon(h_q\hat{d}_q)^2]\delta_{im}\hat{d}_n\hat{d}_j d\Omega(D_{mn} + R_{mn}) = 0 \tag{B1}$$

or

$$\begin{aligned} & \varepsilon_{kij}\left[\frac{(5-2\epsilon)}{15}\delta_{nj}\delta_{im} + \frac{6\epsilon}{15}\delta_{im}h_n h_j\right]R_{mn} \\ & \quad = -\varepsilon_{kij}\frac{2\epsilon}{5}\delta_{im}h_n h_j D_{mn}. \end{aligned} \tag{B2}$$

With Eq. (A4), Eq. (B2) becomes

$$R_{mn} = \frac{3\epsilon}{5+\epsilon}\varepsilon_{msn}\varepsilon_{spj}h_k h_j D_{pk}. \tag{B3}$$

APPENDIX C

The solutions of the integrals of our interest are

$$\begin{aligned} I_1 = {} & \frac{4c^{3/2} - 2bc^{1/2}}{8c^{3/2}}(b+c)^{1/2} \\ & + \frac{4bc + b^2}{8c^{3/2}}\log\left(\frac{\sqrt{b+c} + c^{1/2}}{\sqrt{b+c} - c^{1/2}}\right) \end{aligned} \tag{C1}$$

and

$$\begin{aligned} I_2 = {} & \frac{4c^{3/2} + 2bc^{1/2}}{8c^{3/2}}(b+c)^{1/2} \\ & + \frac{b^2}{8c^{3/2}}\log\left(\frac{\sqrt{b+c} - c^{1/2}}{\sqrt{b+c} + c^{1/2}}\right). \end{aligned} \tag{C2}$$

[1] J. Jenkins, D. Johnson, L. La Ragione, and H. A. Makse, J. Mech. Phys. Solids **53**, 197 (2005).
[2] L. La Ragione and J. T. Jenkins, Proc. R. Soc. London, Ser. A **463**, 735 (2007).
[3] K. Johnson, *Contact Mechanics* (Cambridge Press, Cambridge, 1985).
[4] V. Nardelli and M. R. Coop, Procedia Eng. **158**, 39 (2016)
[5] Y. C. Chen, I. Ishibashi, and J. T. Jenkins, Geotechnique **38**, 25 (1988).
[6] I. Ishibashi, T. K. Agarwal, and S. A. Ashraf, *International Conference on First Discrete Element Methods, Golden, CO* (Colorado School of Mines, Golden, CO, 1989).
[7] C. Thornton and S. J. Antony, Philos. Trans. R. Soc. London A **356**, 2763 (1998).
[8] I. Agnolin and J. N. Roux, Phys. Rev. E **76**, 061304 (2007).
[9] P. A. Cundall and O. D. L. Strack, Geotechnique **29**, 47 (1979).
[10] O. I. Imole, M. Wojtkowski, V. Magnanimo, and S. Luding, Phys. Rev. E **89**, 042210 (2014).
[11] N. P. Kruyt and L. Rothenburg, Acta Mech. **225**, 2301 (2014).
[12] S. Luding, Gran. Mat. **10**, 235 (2008).
[13] I. Agnolin, J. T. Jenkins, and L. La Ragione, Mech. Mat. **38**, 687 (2006).
[14] I. Agnolin and N. P. Kruyt, Comp. Math. Appl. **55**, 245 (2008).

[15] L. La Ragione and J. T. Jenkins, J. Mech. Phys. Solids **57**, 1449 (2009).
[16] J. T. Jenkins and O. D. L. Strack, Mech. Mater. **16**, 25 (1993).
[17] A. Ezaoui and H. Di Benedetto, Geotechnique **59**, 621 (2009).
[18] L. La Ragione and L. Oger, Phys. Rev. E **86**, 041309 (2012).
[19] L. La Ragione and V. Magnanimo, Gran. Mat. **14**, 749 (2012).
[20] S. Luding, Int. J. Sol. Str. **41**, 5821 (2004).
[21] L. La Ragione, V. C. Prantil, and I. Sharma, Int. J. Plast. **24**, 168 (2008).
[22] M. Oda, Soils and Found. **1**, 17 (1972).
[23] P. E. Peyneau and J. N. Roux, Phys. Rev. E **78**, 041307 (2008).
[24] N. Kumar, S. Luding, and V. Magnanimo, Acta Mech. **225**, 2319 (2014).
[25] L. La Ragione, L. Oger, G. Recchia, and A. Sollazzo, Proc. R. Soc. A **471**, 2183 (2015).
[26] L. La Ragione, V. C. Prantil, and J. T. Jenkins, J. Mech. Phys. Solids **83**, 146 (2015).